Chapter 18

Development and Applications of the ARM Raman Lidar

D. D. TURNER

NOAA/National Severe Storms Laboratory, Norman, Oklahoma

J. E. M. GOLDSMITH

Sandia National Laboratories, Livermore, California

R. A. FERRARE

NASA Langley Research Center, Hampton, Virginia

1. Introduction

From the earliest days of the Atmospheric Radiation Measurement (ARM) Program, measurements of water vapor profiles at high temporal and vertical resolution were deemed to be critical for both the radiative transfer and cloud processes studies that the ARM Program planned to undertake (DOE 1990). The dream of the ARM Program founders was that ground-based remote sensors would measure these profiles routinely, and that the program would be able to move away from the routine launching of radiosondes to characterize the thermodynamic profile above the ARM sites. This is reflected in the original program plan, in which the first two profiling systems listed were Raman lidar or differential absorption lidar (DIAL) to profile water vapor, and radio acoustic sounding systems with radar wind profiles to measure temperature and wind profiles (DOE 1990).

Here, we discuss the history of using lidars to profile water vapor within the ARM Program, including the early studies to determine what type of lidar would be best suited for the program, the development of the ARM Raman lidar, the initial challenges that were experienced with the construction of the first fully automated system, and examples that demonstrate the scientific utility of the ARM Raman lidar.

Corresponding author address: D. D. Turner, NOAA/National Severe Storms Laboratory, Forecast Research and Development Division, National Weather Center, 120 David L. Boren Blvd., Norman, OK 73072.
E-mail: dave.turner@noaa.gov

DOI: 10.1175/AMSMONOGRAPHS-D-15-0026.1

2. Using lidars to profile water vapor before ARM

The development of the laser in the early 1960s led to much excitement in the scientific community, and it was not long before the laser was used to study the atmosphere. This was especially true after the development of reliable lasers that were able to emit high-energy, short (~ns) pulses of narrowband radiation. The first lidar remote sensing experiment that used these new lasers was used to determine the distance between Earth and the moon (Smullin and Fiocco 1962).

Raman lidars take advantage of the Raman energy shift that occurs when a photon scatters inelastically off a molecule in the atmosphere, resulting in a lower energy (longer wavelength) photon. The energy shifts associated with this process are molecule specific and are relatively large (e.g., the vibrational-rotational shifts are 3652 and 2331 cm^{-1} for water vapor and nitrogen, respectively); this makes the selection of the return from various molecules relatively easy using dichroic beam splitters and interference filters. The first Raman lidar measurements occurred in 1966, as measurements of nitrogen (Cooney 1968) and oxygen (Leonard 1967)—the gases with the highest concentrations in the atmosphere—were made. The first Raman lidar water vapor measurements of the atmosphere were made in 1969 by Harvey Melfi, who showed good agreement with coincident radiosonde profiles of water vapor (Melfi 1972). Turner and Whiteman (2002) provide a history of using Raman lidars to profile trace gases and aerosols in the atmosphere.

DIAL systems profile water vapor in a different manner. DIALs transmit laser energy at two wavelengths: one

tuned to the absorption line of the gas of interest, and one at a nearby wavelength where the absorption by that gas is markedly smaller. In these systems, the laser beam is typically scattered back to the system by aerosol particles, since the wavelengths used are typically in the near-infrared where molecular scattering is very weak. The analysis then proceeds to measure the amount of relative attenuation that occurred between the online and offline returns, and since the relative strengths of the absorption at the two wavelengths is known, the concentration of the gas at each range cell can be determined. Ed Browell and his colleagues (Browell et al. 1979) were among the pioneers who profiled water vapor and ozone using ground-based and airborne DIAL systems.

The invention of the laser led to an intense period of activity as the laser was utilized to probe the atmosphere. However, lasers were still immature and detectors were inefficient. Raman scattering is a very weak process (approximately 3–4 orders of magnitude smaller than Rayleigh scattering), and thus the signal-to-noise ratio hampered many atmospheric studies using this technique. The stringent requirements of frequency control on the online wavelength made the laser transmitters in DIAL systems extremely complicated, and hindered their development. It was not until the late 1980s, when higher-power and better-quality lasers were developed as well as greatly improved detection technologies, that the atmospheric Raman lidar and DIAL observations regained the "luster" they had in the late 1960s and early 1970s.

The advances in both laser and detector technology in the mid-to-late 1980s led to a rebirth of the lidar atmospheric sensing of water vapor. For example, Harvey Melfi and his group at the National Aeronautics and Space Administration (NASA) Goddard Space Flight Center (GSFC) used Raman lidar measurements to provide detailed information on the structure of water vapor during frontal passages (Melfi et al. 1989) and some airborne DIAL systems were being developed at this time (e.g., Ehret et al. 1993; Ismail and Browell 1989). However, because of the weak Raman scattering process and high solar noise during the daytime, Raman lidars were only used at night. Furthermore, both Raman lidars and DIAL systems were still manually intensive research instruments, and only small, sporadic datasets were being collected. Thus, the ARM Program had two viable options and needed to determine which of the two avenues would more likely lead to a successful automated system.

3. The decision process

Measuring the evolution of water vapor in the boundary layer over the entire diurnal cycle was deemed to be a critical measurement for the ARM Program. The two technologies, Raman lidar and DIAL, both had attractive features yet both also had some drawbacks. The primary strengths and weaknesses, in a relative sense, are listed in Table 18-1 and were also provided in a review article by Grant (1991); a survey of the accuracy and resolution of different Raman lidars and DIAL systems was provided in Weckwerth et al. (1999). A proposal to pursue both technologies was submitted to the ARM Instrument Development Program (Stokes 2016, chapter 2), but the complexity of the DIAL laser transmitter and concerns about its stability, which must be frequency-stabilized to a selected water vapor absorption line, led to a decision to only fund the Raman lidar work as a collaboration between Sandia National Laboratories (SNL) and the GSFC group.

TABLE 18-1. Relative advantages of the Raman lidar vs DIAL, as perceived in the early 1990s.

System	Advantages
Raman lidar	Simpler laser transmitter Able to profile aerosol extinction and backscatter directly (without assumptions) Higher nighttime maximum altitude limit
DIAL	Better signal-to-noise in boundary layer No need for external calibration standard

However, this decision then led to additional questions. Raman lidars measure the energy shift associated with Raman scattering by water vapor and nitrogen molecules, and the strength of this scattering is proportional to λ^{-4}, where λ is the wavelength of the laser. Thus, the shorter the wavelength of the laser, the more intense the Raman scattering signal is (all other things equal), which is an advantage since Raman scattering is a weak process. Photomultiplier detectors are also more efficient and have lower background levels at shorter wavelengths.

Therefore, lasers that operate in the UV are desirable. There were two choices:

1) Should the program use a solid-state or excimer (gas) laser?
2) What was the best system configuration to maximize performance in the daytime where there would be significant background signal from the sun?

Excimer lasers were relatively popular in the early 1990s because they had higher output power levels than solid-state lasers. Initial Raman lidar development within the ARM Program evaluated, among other things, different types of excimer lasers (Goldsmith et al. 1994). However, the gases used within these lasers were corrosive and difficult to handle. Additionally, the beam quality was poorer for excimer lasers than for solid-state lasers;

this is important if the detector uses a narrow field of view (FOV). For these reasons, the ARM Program ultimately elected to use a solid-state neodymium-doped yttrium–aluminum–garnet (Nd:YAG) laser in its operational system.

Two studies proceeded simultaneously by groups at SNL and GSFC to evaluate the best system configuration to make daytime Raman lidar water vapor measurements. GSFC investigated making water vapor observations in the so-called solar-blind region of the spectrum (Whiteman et al. 1993), where the laser transmitted in a spectral region of the UV (248 nm) and there was significant absorption of the solar energy by ozone, which reduced the solar signal measured by the detectors; this approach had been used in the late 1970s (Renaut et al. 1980). SNL investigated the use of a very narrow FOV with narrow interference filter bandpasses for the receiver to reduce the amount of solar background (Bisson and Goldsmith 1993), using a laser that operated at 308 nm where ozone absorption is minimal in the troposphere. Note that the narrow bandpass interference filters utilized very new technology in order to maintain a reasonable transmission, and there were concerns about leakage of out-of-band radiation that would contaminate the measurements. These studies helped to confirm a modeling study that indicated both solar-blind and narrow bandpass/narrow FOV systems had similar daytime capabilities (Goldsmith and Ferrare 1992).

The initial studies demonstrated fairly rapidly that the narrow bandpass, narrow FOV system offered similar range capability as the solar blind method during the day, but was more accurate because the differential absorption of ozone in the boundary layer did not need to be determined. Furthermore, the narrow bandpass, narrow FOV systems were much superior during the nighttime, allowing water vapor to be profiled throughout the troposphere. However, there were still questions to be answered regarding the optimization of the configuration of the systems, and thus personnel at both GSFC (Whiteman et al. 1992) and SNL (Bisson et al. 1999) built systems to investigate these issues. These two systems were then deployed side by side and numerous radiosondes, which served as truth, were launched in order to evaluate the different technologies (Goldsmith et al. 1994). The SNL ''big lidar'' served as the prototype for the Cloud and Radiation Testbed (CART) Raman lidar (CARL), while the GSFC scanning Raman lidar (SRL) provided extremely useful observations in future water vapor campaigns (Turner et al. 2016, chapter 13) and evolved with time over the next decade, serving as an experimental platform for subsequent upgrades to CARL.

4. Development and evolution of the ARM Raman lidar

a. Building the Raman lidar

The results from all of these studies were used in the development of the operational CART Raman lidar. The lidar would use a solid-state Nd:YAG laser (output at 355 nm) and a narrow bandpass, narrow FOV architecture. To improve the observations in the near field (i.e., in the lowest several hundred meters just above the Raman lidar), the lidar would have a second FOV that had a larger aperture and would make measurements simultaneously with the narrow FOV. The narrow and wide FOV of the lidar would be set to 0.3 and 2 mrad, respectively; these are often referred to as the high-altitude (or high) and low-altitude (low) channels. All channels would use interference filters that had a nominal bandpass of 0.3 nm. The full details of the CARL system are given in Goldsmith et al. (1998).

The Raman lidar community had demonstrated that aerosol extinction could be measured directly by a Raman lidar system without the need for any assumptions relating aerosol backscatter to extinction (Ansmann et al. 1990), and a number of experimental Raman lidar systems were built with the capability to measure both water vapor and aerosol extinction (e.g., Whiteman et al. 1992; Ansmann et al. 1992; Reichardt et al. 1996). Thus, both FOVs in the aft optics of the operational Raman lidar would be configured with channels sensitive to the vibrational-rotational Raman scattering by water vapor (408 nm) and nitrogen (387 nm), as well as channels sensitive to the elastic return at the laser wavelength (Fig. 18-1, top). Thus, two lidar systems would share the same laser transmitter and telescope. This redundancy in the aft optics would prove to be useful in later analyses.

To make this an autonomous system, it would be necessary to monitor and adjust several parameters that were formerly performed manually. In particular, the laser output power and the alignment of the outgoing laser beam within the narrow FOV fluctuated with the temperature inside the enclosure due to thermal expansion and vibrations; it would be necessary to develop automated ways to maintain the optimal alignment of each of these components.

Routines were developed in LabView (the software that ran the CARL system) to optimally adjust the alignment of the frequency doubler and trippler crystals within the laser, thereby maintaining maximum laser output power, and the orientation of the final steering mirror that directed the laser beam into the sky. These routines were run at regular intervals (e.g., every 3 h) to ''tweak'' the laser power or alignment. During each alignment tweak, the system would stop collecting data

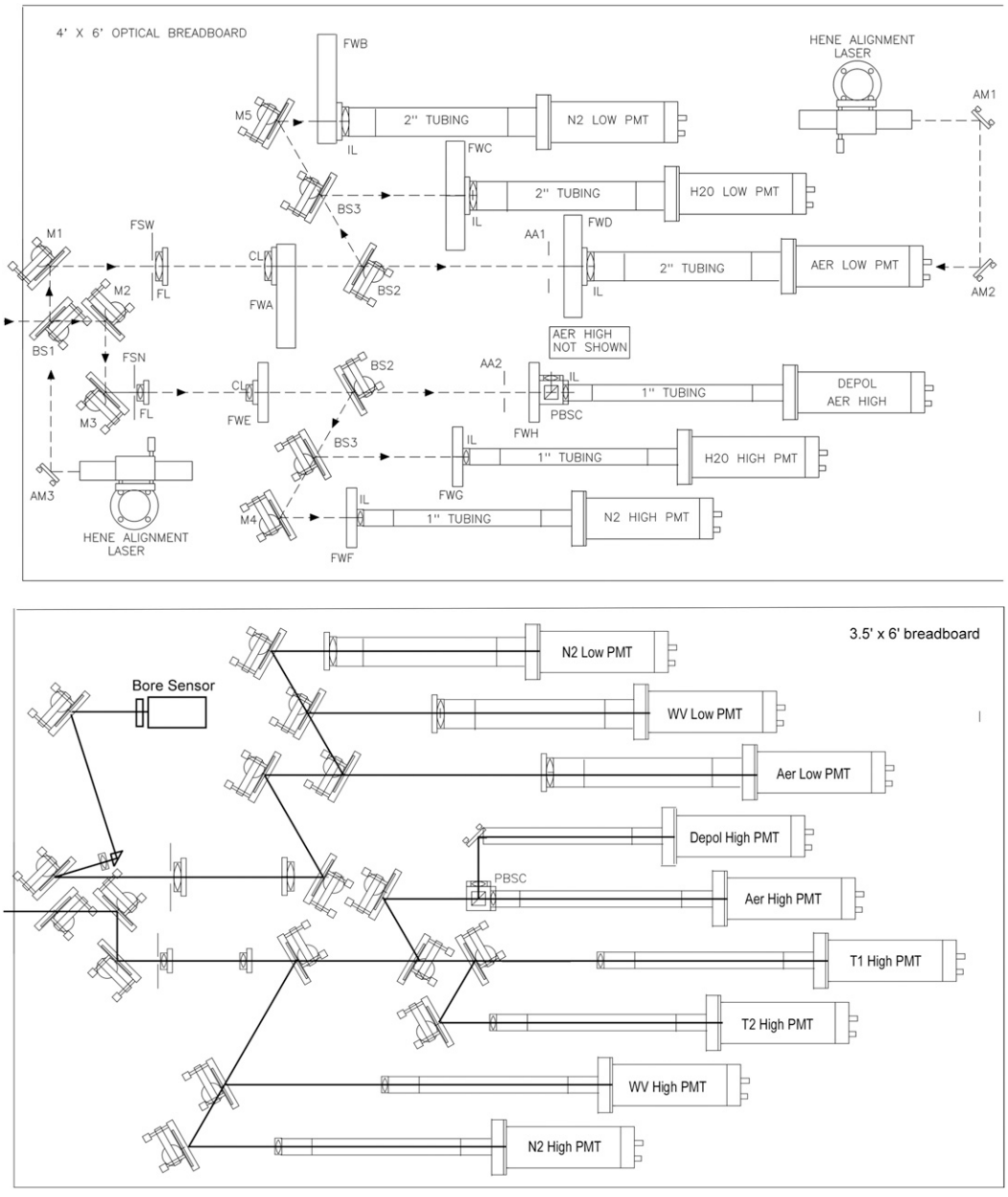

FIG. 18-1. The layout of the aft optics of the ARM Raman lidar (top) as originally deployed in 1996 and (bottom) after the 2004 upgrade. The receiver telescope is located to the left of the optical breadboard, with the light coming into the aft optics through beam splitter ''BS1'' (only identified in the top layout).

momentarily, and then scan the laser beam through the FOV along the north–south axis, fit a polynomial to the data, and then return to the location that maximized the return signal. The process was then repeated along the east–west axis, and then the system would return to operations. Ideally, this would align the laser within the center of the FOV; however, in practice hysteresis in the micromotors that moved the mirror would result in some minor amount of misalignment. This would turn out to have a negligible effect on the derived water vapor mixing ratio, but would be a serious challenge to the aerosol processing scripts for reasons described below. Note that a similar tweaking strategy was used to optimize the orientation of the doubling and tripling crystals within the laser.

While the alignment tweak logic typically worked well in clear skies, the presence of clouds, especially if a cloud advected over the lidar during the tweak process, could

result in very poor results. Thus, the LabView software needed to have logic built into it to identify clouds before the tweak process occurred and abort it. The software also needed to identify periods when the tweak was unsuccessful for any reason (typically due to clouds); if this occurred then the software needed to be able to return to the original alignment position and continue making measurements. This procedure usually worked well, but occasionally the system would end up misaligned. If the misalignment was not bad, then the next alignment tweak would correct it; however, on the rare occasions it would be necessary for the operators at the Southern Great Plains (SGP) site to manually restore the alignment. (These situations where the operators needed to perform a manual adjustment were easily determined by eye in cloud-free conditions because the raw signal in the narrow FOV nitrogen channel would decay too quickly with height.)

It was essential for an operational system to be eye-safe. CARL operates in the UV region of the spectrum where the maximum permissible exposure (MPE) is higher than in the visible or near-infrared portion of the spectrum. However, since Raman scattering is such a weak signal, CARL uses a high-energy laser that transmits 300–400 mJ pulses at 30 Hz. This could only be achieved by expanding the laser beam significantly to reduce the energy density of the outgoing beam. This was done with a 15× beam expander prior to the final steering mirror. Calculations indicated that any aircraft overhead would have to be flying slower than 6 miles per hour in order to exceed the MPE at any point. This eliminated the need to have a manual spotter or automated radar to disable the system if an aircraft passed above the lidar (Goldsmith et al. 1998).

While CARL was an automated system, there were three things that greatly reduced its operational uptime after it was initially deployed in the mid-1990s. The first issue was the threat of hail; a large hailstone could easily shatter the protecting window above the telescope and thus the telescope itself. Thus, site operations staff shut down CARL and closed its hardened hatch whenever severe weather was imminent; the threat of weather like this occurs relatively often in north-central Oklahoma. In the spring of 1998, a stainless steel wire mesh was placed above the output window to protect the system from hail, which allowed continuous lidar operations in these weather conditions. The installation of the hail shield decreased the strength of the backscattered signal by about 18%, but this was deemed to be acceptable in order to maintain a higher uptime without the risk to the system.

The second issue that affected operational uptime was power continuity. Small disruptions in electrical service, even for a fraction of a second, would cause the laser to shut down. The laser could not be restarted automatically, and required manual intercession to physically turn a key to restart the system. Murphy's Law would dictate that these power bumps would happen most in the evenings or on weekends when the SGP operators where not on site, and resulted in significant periods of downtime. This issue was solved with the installation of a large uninterruptible power supply that conditions the power for the lidar and is able to run the system for several minutes in the event of a power fluctuation. These changes, as well as a variety of other minor system improvements (e.g., improvements in the air conditioning system in the lidar's enclosure, continued improvement of the laser and its components by the vendor, etc.), led to a continued increase in the operational uptime as the lidar matured (Fig. 18-2).

The ARM Program realized early on that it would need scientific experts to serve as ''mentors'' for the various instruments in the program. These mentors would provide guidance for the site operations staff and help develop analysis techniques to improve the use of the data from their system throughout the program. The Raman lidar was the first ARM instrument to have a dual-mentor model, wherein one mentor was responsible for the hardware/system aspects of the instrument and the second mentor was responsible for the development of analysis routines and calibration. This model has been highly successful and is still used within ARM today both for the Raman lidar and other instruments (e.g., the millimeter cloud radar).

b. Measuring water vapor

The Raman lidar was delivered to the SGP site during the fall of 1995, but it took many months before the system was truly ready to collect data. During this period, the Instantaneous Radiative Flux (IRF) working group organized a series of water vapor intensive operational periods (WVIOPs) that would, in part, help to evaluate the accuracy of the Raman lidar's water vapor measurements. The IRF working group was extremely interested in getting remotely sensed profiles of water vapor in order to improve their radiative transfer models, because the uncertainty in the radiosonde water vapor profiles was the limiting factor in improving the accuracy of clear-sky infrared radiative transfer models at the time (Revercomb et al. 2003). The first two WVIOPs, which were conducted in the fall of 1996 and 1997, brought a wide range of instruments to the SGP site, including the SRL from GSFC, tethersondes and aircraft measuring water vapor in situ, and other instruments. These datasets were used to develop an automated calibration strategy for the CARL and to

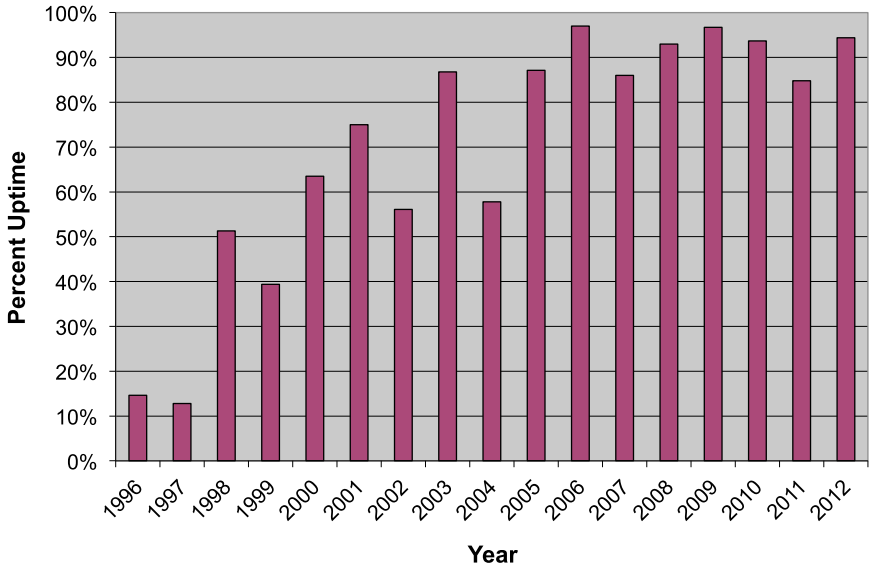

FIG. 18-2. Operational "uptime" of the SGP Raman lidar (CARL) per year.

evaluate the accuracy of this calibration over the diurnal cycle.

Raman lidar water vapor profiles normally are calibrated to an external measurement of water vapor, due to uncertainty in the Raman backscattering cross section of water vapor and difficulties associated with characterizing the wavelength dependence of the system throughput. Prior to these WVIOPs, the most common calibration standard was the radiosonde; the Raman lidar profile would be calibrated using a height-independent scale factor to match the radiosonde measurements over some altitude region. However, one of the main findings of the WVIOPs (Revercomb et al. 2003; Turner et al. 2003) was that the calibration of the radiosonde's water vapor sensor can vary significantly between calibration batches, and also changed with the age of the radiosonde (i.e., the time period between when the sonde was calibrated in the factor to when it was actually launched into the atmosphere). Furthermore, Ferrare et al. (1995) had demonstrated that some types of radiosondes have very poor performance in low relative humidity conditions (RH $<$ 30%), and using these data would result in very poor calibration for the Raman lidar. These calibration uncertainties were the source of the IRF's frustrations with radiosondes. Thus, a different calibration standard for the Raman lidar was needed.

The WVIOPs demonstrated that the microwave radiometer (MWR) observed precipitable water vapor (PWV) value was much more robust and accurate than the corresponding value-derived radiosonde water vapor data (Turner et al. 2016, chapter 13), and a decision was made to calibrate CARL against this measurement. During the night in clear-sky scenes, this was perfectly acceptable because CARL was able to profile water vapor from near the surface (the in situ observations from the surface and 60-m tower were used to fill in the lowest levels where the lidar was blind) to above 10 km with only a 10-min average; thus the lidar was seeing over 99% of the water vapor in the column and comparisons with the MWR could be performed. However, in cloudy scenes where the laser beam was attenuated, or in the daytime when the solar noise limited the maximum altitude of the lidar water vapor observations to about 3 km, a different approach was needed. Furthermore, in order to prevent saturation of the detectors in the 408-nm water vapor channels, the lidar used a "bright" mode during the daytime, wherein the lidar automatically inserted neutral density filters into these channels to attenuate the signal. Thus, it was not obvious originally how to transfer the nighttime calibration into the daytime.

The approach that was initially used was to determine separate calibration factors for the nighttime and daytime periods, where the latter used an estimate of the fraction of the PWV that the lidar did see (based upon a radiosonde climatology relating fraction of PWV to height above the surface) to scale the MWR-derived PWV to the lidar value (Turner and Goldsmith 1999). This initial approach yielded acceptable intercomparison results between the lidar and radiosondes, in situ observations from tethersondes, and aircraft observations. However, the approach also demonstrated some large errors (5%–10%) at sunrise and sunset in the 1996 WVIOP results (Turner and Goldsmith 1999). It was

believed that these errors were due to nonlinear effects in the lidar detection system, and a variety of different correction factors were unable to satisfactorily remove the error. A simple change of switching to (from) the bright mode earlier (later) in the day at sunrise (sunset) was tested in the 1997 WVIOP and showed marked improvements.

However, these comparisons still did not yield great faith in the consistency of the nighttime versus daytime calibration of CARL's water vapor measurements. The WVIOPs did demonstrate conclusively that the CARL and SRL systems agreed to better than 5% in water vapor mixing ratio if using the same data source for their height-independent calibrations (Revercomb et al. 2003), which was an excellent result as there are a range of lidar-dependent correction factors that need to be applied to the data (e.g., corrections for photon pulse-pileup, overlap, etc.). To evaluate the consistency of the night-vs-day calibrations, the water vapor DIAL from the Max Planck Institute for Meteorology (Wulfmeyer and Bösenberg 1998) was deployed to the SGP site in 1999 for the so-called lidar WVIOP. The comparison of the DIAL with CARL demonstrated that the method of calibrating the daytime and nighttime data independently resulted in an approximate 10% diurnal bias in the Raman lidar calibration (Linne et al. 2000). We also realized that we could simply translate the nighttime calibration factor into the daytime by simply accounting for the attenuation of the bright mode neutral density filter; this made the daytime and nighttime data fully consistent.

Since CARL is an automated system, we needed to be able to calibrate data when an evening was cloudy and there had to be consistency in calibration for consecutive days. Thus, an approach was adopted that used nighttime data from three consecutive days to determine the calibration factor for the central day (Turner et al. 2002). This rolling calibration approach would also be used for calibrating other CARL data products.

The water vapor profiles in the boundary layer and midtroposphere were used in several different studies. In the first example, the CARL observations were used to evaluate the accuracy of the water vapor profiles retrieved from the Atmospheric Emitted Radiance Interferometer (AERI) when the structure of the boundary layer was evolving rapidly, such as during the passage of atmospheric fronts or drylines (Turner et al. 2000). CARL data were also used in the evaluation of infrared radiative transfer models during clear-sky periods (Turner et al. 2004); however, lack of coincident temperature profiles from a measurement system other than the radiosonde proved to be a limiting factor in this application. Another interesting application used CARL water vapor observations to investigate horizontal convective rolls in the convective boundary layer (Mecikalski et al. 2006); this would be the first paper of several that would start to take advantage of the high temporal and spatial resolution of the Raman lidar observations to look at boundary layer structure and phenomena.

The advances from the 1996, 1997, and 2000 WVIOPs demonstrated that CARL is able to measure water vapor well in the boundary layer and midtroposphere, but how well could it measure water vapor in the upper troposphere (UT) at night? To answer this question, and to evaluate that accuracy of other water vapor measurements in the UT, ARM and NASA conducted the ARM–FIRE Water Vapor Experiment (AFWEX) over the SGP site in late 2000. Like the previous WVIOPs, the GSFC SRL was deployed near CARL, but AFWEX also benefited from the deployment of the airborne NASA Langley Research Center Laser Atmospheric Sensing Experiment (LASE) water vapor DIAL (Browell et al. 1997) on the NASA DC-8 aircraft and the launching of chilled mirror frostpoint hygrometers during the campaign. AFWEX demonstrated very good agreement between CARL, SRL, and LASE throughout the entire troposphere (Ferrare et al. 2004). AFWEX analyses also demonstrated that Vaisala RS80-H radiosondes (the model being launched by the ARM Program at the time) had a significant dry bias (10%–30%) in the UT, but that a known radiosonde calibration model correction and accounting for the time lag of the sonde sensor removed this bias (Ferrare et al. 2004). These nighttime comparisons provided high confidence in the CARL observations of humidity throughout the troposphere, and set the stage for a couple of interesting UT projects.

The large dry bias in the radiosonde UT data has significant implications for outgoing longwave radiation calculations and modeling (e.g., Ferrare et al. 2004), satellite radiance and product validation, and modeling studies investigating cirrus processes and properties. However, CARL was only at a single location, and thus there was a desire to transfer the knowledge acquired during AFWEX to a larger domain. Soden et al. (2004) compared nighttime measurements from CARL, the radiance observations in the 6.7-μm water vapor channel on the Geostationary Operational Environmental Satellite (*GOES-8*), and radiosonde profiles over a multimonth period that encompassed all of the WVIOP periods. This was the extension of an earlier work that used the NASA SRL observations collected during the FIRE campaign in Coffeyville (Soden et al. 1994). Using a simple model to convert between radiance space and profile space, they showed that the GOES and

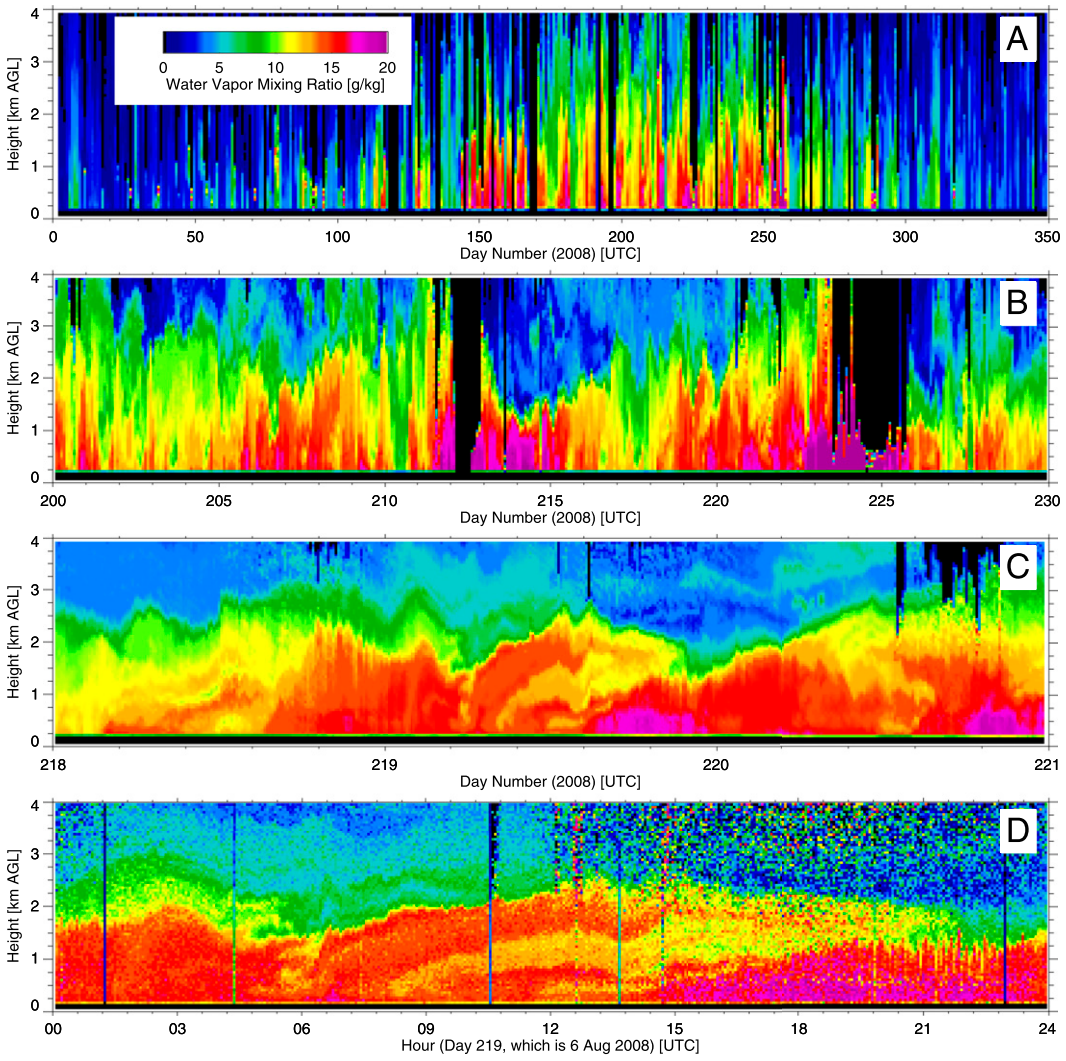

FIG. 18-3. Raman lidar water vapor mixing ratio time–height cross sections for data collected in 2008 at the SGP, with a range of different "zooms": (a) 350 days, (b) 30 days, (c) 3 days, and (d) 1 day. The data in the first three panels are at 10-min, 75-m resolution, whereas the resolution of the data in (d) is 10 s, 37.5 m.

Raman lidar observations agreed to within 10%, but that the radiosonde was systematically drier by ~40%. The authors then developed a variational assimilation method that used GOES radiances to correct the radiosonde dry bias, demonstrated its accuracy, and discussed the utility of this method to correct radiosondes launched at other locations beyond the SGP.

Cirrus clouds play an important role in both the energy and moisture budgets of the atmosphere. Upper tropospheric humidity plays an important role in the nucleation (i.e., homogeneous vs heterogeneous nucleation) and maintenance of cirrus clouds, yet is a difficult variable to measure for long periods of time across a range of conditions. Comstock et al. (2004) used a year of CARL UT water vapor observations to demonstrate that ice supersaturation occurs more than 40% of the time in the uppermost portions of midlatitude cirrus clouds, which supports the theory that homogeneous nucleation occurs frequently.

c. Measuring aerosol properties

The automated nature of the Raman lidar provided wonderful multiday views of water vapor mixing ratio (e.g., Fig. 18-3) and aerosol scattering ratio and extinction (Fig. 18-4). The initial analysis of the aerosol data showed tremendous promise in the observations, but there were some artifacts in the data. The ARM Raman lidar was designed to measure water vapor first and foremost; aerosol and cloud observations were considered of secondary importance. This ultimately led to

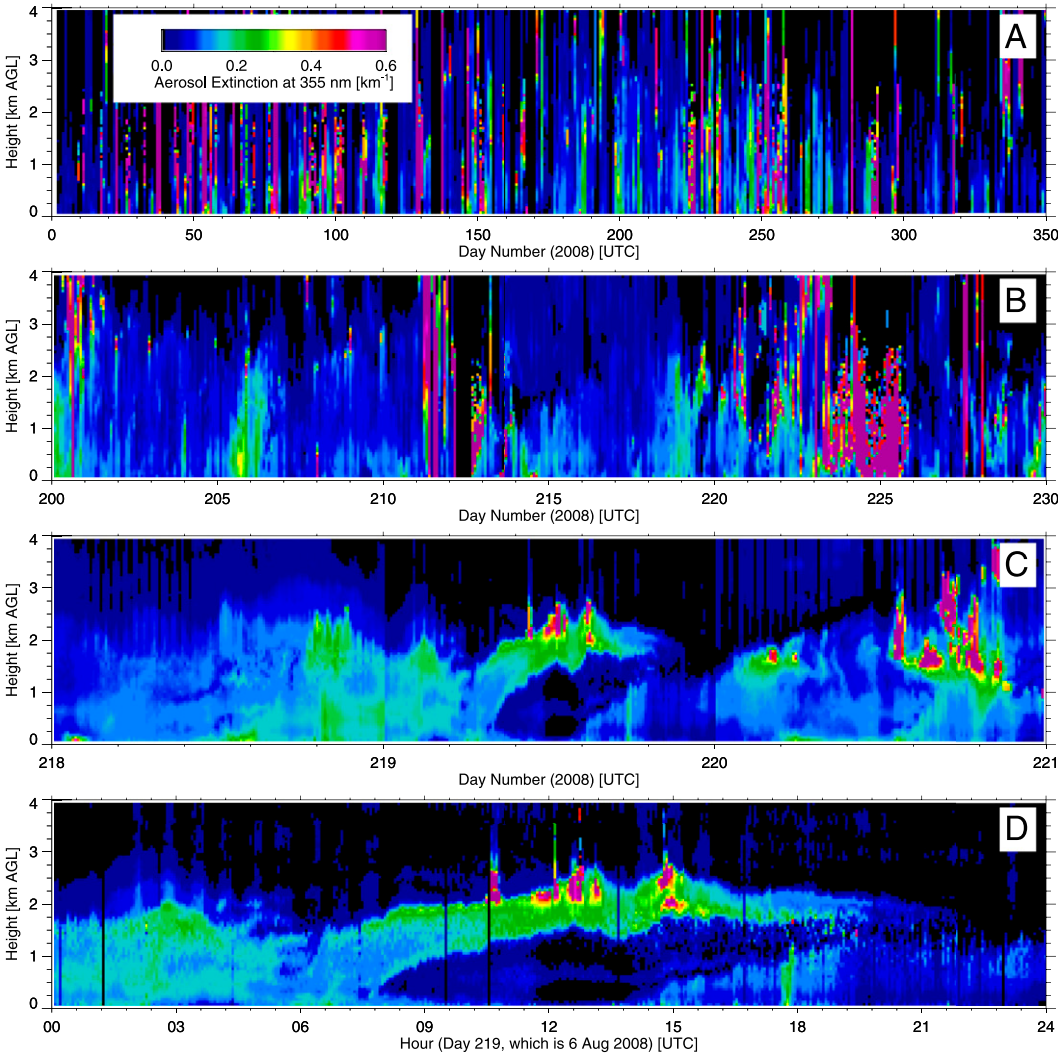

FIG. 18-4. (a)–(d) Raman lidar aerosol extinction time–height cross sections for the same time periods as shown in Fig. 18-3. The temporal resolution of (a)–(c) is 10 min, whereas the temporal resolution in (d) is 1 min. Areas of high extinction (purple) are primarily due to extinction by clouds.

some design choices in the construction of CARL that would turn out to hinder the derivation of aerosol scattering ratio (and hence backscatter coefficient) and extinction coefficient from the data.

The main ''problem'' was the orientation of the co-polarized elastic return (i.e., the channel sensitive to the return at 355 nm) in the narrow FOV (henceforth called the high aerosol channel). The layout of the aft optics for the system in circa 1996 is shown in the top of Fig. 18-1. The separation of the co- versus cross-polarized elastic return was done with a polarizing cube, and thus the co- versus cross-polarized light would leave this optical element at positions 90° angles from each other. Because of space limitations on the optical breadboard, the high aerosol channel was oriented normal to the optical table (i.e., sticking up in the air). However, this made the channel susceptible to vibrations in the lidar enclosure (such as when the outer door was shut) and also thermal variations that were different than the other channels. Thus, the periodic alignment tweaks affected the alignment of this particular channel differently than the other channels that were all lying flat on the optical table.

The automated analysis software, which is run in a postprocessing mode in the ARM Data Management Facility, needed a solution. The approach used the wide FOV aerosol scattering ratio (ASR), which is defined as the ratio of the elastic return divided by the nitrogen return that has been calibrated to be unity in aerosol-free air, to determine the overlap correction for the narrow FOV (Turner et al. 2002). Each alignment tweak

period was treated independently, and this approach (after numerous attempts to bullet-proof the routines) led to accurate ASR profiles throughout the troposphere. The same approach was used to correct for the overlap in the narrow FOV nitrogen channel, and thus allow the derivation of aerosol extinction profiles from the narrow FOV nitrogen data, which is less noisy than the wide FOV data (Turner et al. 2002).

The automated measurements of aerosol extinction and water vapor mixing ratio were new for the scientific community; up to this point, all Raman lidars were operated in episodic fashion, typically by a dedicated group of lidar scientists and engineers. The operational nature of CARL allowed a large dataset to be quickly collected, which led to the first climatologies of aerosol extinction and water vapor from Raman lidar (Turner et al. 2001). Furthermore, since Raman lidars can simultaneously measure aerosol extinction and backscatter coefficients directly (the latter is easily derived from the ASR profile), studies on the variability of the ''lidar ratio,'' which is the ratio of the extinction to backscatter coefficients, could be performed. The lidar ratio is an intensive property of the aerosols and is sensitive to aerosol size, composition, and shape. The lidar ratio was usually assumed to be constant in order to derive aerosol extinction from single wavelength lidars, such as the ARM micropulse lidar (Campbell et al. 2002). Ferrare et al. (2001) showed for the first time that this was often a poor assumption over the central part of the United States, with approximately 30% of CARL observations showing significant changes in the lidar ratio as function of height. The aerosol data from the Raman lidar were very useful in characterizing different aerosol layers over the SGP site when smoke from fires in Central America advected over the SGP site (Peppler et al. 2000).

In the late 1990s, ARM began to place more emphasis on characterizing the aerosol properties above its sites (McComiskey and Ferrare 2016, chapter 21). Earlier work, supported both by the program (e.g., Kato et al. 2000) and by others (e.g., Masonis et al. 2002), demonstrated that Raman lidar measurements of aerosol extinction were typically 30% larger than airborne in situ measurements. To resolve this discrepancy and more completely describe the aerosol optical, microphysical, and chemical properties above the SGP site, the ARM Program conducted the aerosol IOP in May 2003 (McComiskey and Ferrare 2016, chapter 21). This experiment would bring a large array of aerosol instruments to the site to complement the routine ARM observations and would be one of the most expensive IOPs conducted by the ARM Program at the time.

Unfortunately, CARL had problems during this IOP. The system had been experiencing a slow degradation of its sensitivity starting in early 2002, and this degradation was not noticed until after this IOP. The impacts on the data quality were significant, as the random noise level had increased by a factor of 2–4 from its baseline values in the late 1990s by the time of the aerosol IOP, depending on the data product (Ferrare et al. 2006). The higher noise level reduced the maximum range of the aerosol and water vapor profiles, and greatly impacted the ability of the automated aerosol routines to correct for alignment issues in the narrow FOV with the wide FOV data. Because of the importance of the aerosol IOP, a massive analysis effort was made by Ferrare and Turner to advance the logic in the automated scripts in order to handle the adverse effects of the noisier raw data (Ferrare et al. 2006). This effort was largely successful, and calibrated data were made available to the IOP participants (albeit with larger error bars than normal).

The reprocessed CARL data were used in a large number of different studies, which testifies to the utility and value of the Raman lidar aerosol and water vapor products. Ferrare et al. (2006) showed that the daytime water vapor measurements were about 5%–10% moister than other observations, and retrievals of single scatter albedo that used CARL lidar ratio values typically agreed well with in situ observations. Schmid et al. (2006) demonstrated that the lidar-observed aerosol extinction and optical depth were still larger than in situ and sun photometer observations, although they expressed hope that if the lidar's sensitivity was its normal value would likely be good agreement between the lidar and sun photometer (this would lead to another field experiment in 2007). Pahlow et al. (2006) used CARL data to characterize the hygroscopic growth of aerosol particles as the relative humidity increases. They showed that the lidar observations are consistent with in situ nephelometer observations, but that the lidar observations can be made over a much higher relative humidity range (i.e., closer to saturation) and do not suffer from as many sampling artifacts experienced by in situ systems. A different study used the CARL observations together with surface in situ measurements to retrieve cloud condensation nuclei concentrations at cloud base (Ghan et al. 2006).

d. Refurbishment and upgrades in 2004

The unanticipated finding of the large degradation in CARL's sensitivity during the analysis of the aerosol IOP stimulated increased activity to identify the source of the problem and correct it. After testing a variety of optical components in both the transmitter and receiver chains, it was concluded that the problem was associated with a decrease in the efficiency of the telescope. The telescope was removed from the system

in the spring of 2004 in order to be refurbished; this process took several months. The installation of the refurbished telescope restored the sensitivity of the lidar to its original levels.

During the early 2000s, a company in Berlin (Licel GbR) developed a new set of detection electronics that combined both analog-to-digital and photon-counting electronics into single package. The two detection systems have different strengths: AD is well suited for large signals (such as those typical for the lower troposphere), but PC is better suited for small signals (such as those in the upper troposphere or from weak scattering processes). The early studies by SNL and GSFC demonstrated that PC detection was superior over most altitude ranges, and hence PC detection was used in the initial development of CARL. The new Licel electronics were first tested in the GSFC SRL (Whiteman et al. 2006), and they worked well and resulted in improved data quality. The Raman lidar instrument mentors decided to switch to the new Licel detection system in CARL; these units were installed into the system while the telescope was being refurbished. Since the combined AD and PC electronics have a larger dynamic range, this allowed the removal of some of the neutral density filters in some channels of the lidar, which were originally in place to prevent the saturation of original PC electronics. The removal of the neutral density filters greatly increased the signal strengths in the aerosol and nitrogen channels by factors of 10–20 (Ferrare et al. 2006), which greatly improved the noise levels of the water vapor and aerosol data products. To properly use the Licel data, the AD and PC datastreams needed to be ''glued'' together, and an automated technique was developed (Newsom et al. 2009).

During that same time period, additional modifications were made. Scientists at GSFC had demonstrated two intriguing new measurements that could be made with a Raman lidar like CARL: (a) atmospheric temperature measurements using rotational Raman scattering by nitrogen and oxygen molecules (Di Girolamo et al. 2004) and (b) measurements of cloud liquid water using Raman scattering (Melfi et al. 1997; Whiteman and Melfi 1999). Thus, the decision was made to add three new channels (two for the rotational Raman scattering and one for liquid water) to CARL. The optical layout of the aft optics after the addition of these new channels is shown in Fig. 18-1 (bottom). Note that when these extra channels were added to the system, the high aerosol and depolarization channels were rearranged so that both of them were lying flat on the optical table just like the rest of the channels. This greatly improved the stability and calibration of the derived aerosol scattering ratio data.

The liquid water Raman measurements were deemed to have a lot of scientific potential because, if they worked, we would be able to measure both cloud and aerosol properties with the same system (same volume and time), which would be beneficial for studying aerosol–cloud interactions. The liquid water Raman scattering cross section is spectrally broad, and thus it was quickly realized that a wide-bandpass filter (6 nm instead of the typical 0.3 nm) would be needed in order to capture scattering across the liquid water Raman spectrum to improve the signal-to-noise ratio. However, the wide bandpass filter was inadequate for the daytime because the solar background over such a large spectral range swamped the signal, and thus the liquid water measurements were only possible during the night. The nighttime liquid water Raman scattering signal was still weak and required five minutes of averaging to get a good signal-to-noise ratio, but during this time the cloud properties changed markedly (even for stratus clouds), making the study of cloud–aerosol interactions problematic. However, Sakai et al. (2013) were able to use these observations to evaluate the strength of the liquid water Raman scattering cross section using AERI data.

Wang et al. (2004) used data from the liquid Raman scattering channel to look at the ice water Raman scattering signal; the liquid water and ice Raman scattering spectra largely overlap in the spectral domain. Wang et al. used these observations to derive ice water content in cirrus clouds, and the technique compared well with more traditional radar–lidar analysis techniques.

The addition of the rotational Raman scattering channels provides an excellent way to get ambient temperature profiles in the same volume as the water vapor mixing ratio, and thus improve measurements such as relative humidity from CARL. However, these channels were only added to the narrow FOV detection system, and thus there were two challenges. The first challenge was that the algorithm would need to use the narrow FOV data much lower to the surface than was done for any the other data products (since we desired temperature profiles over the same range as water vapor data). This made the derived temperature profile very sensitive to alignment of the outgoing laser beam in the detector's FOV. Very quickly, we realized that the 3-hourly alignment tweaks wreaked havoc on the derived temperature profiles. Fortunately, Licel also had developed a very nice and easy-to-use boresight alignment detector, which could be integrated into the Raman lidar system and mated into the LabView software that operated the lidar. This boresight sensor greatly improved the alignment stability of the Raman lidar, and we could use it to continuously maintain the alignment of the system. The accuracy of the aerosol

products were also improved greatly, since the potential for large changes with the older 3-hourly alignment tweaks was eliminated.

The second challenge was how to routinely calibrate the ratio of the rotational Raman lidar signals to provide profiles of ambient temperature. The routine radiosonde launches were used for this purpose. However, the analysis also determined that there was a significant diurnal bias in the calibration that was related to the magnitude of the solar background. An approach was developed that accounts for the solar background in the calibration, thereby providing calibrated data across the diurnal cycle away from radiosonde launch times (Newsom et al. 2013).

The installation of the Licel detection electronics, and the subsequent reduction in the amount of neutral density attenuation in some of the detector channels, opened up a new area of research for the Raman lidar. The maximum temporal resolution for the water vapor mixing ratio and aerosol scattering ratio (and hence backscatter coefficient) was 1 min prior to the upgrade in 2004; the new temporal resolution (having the same approximate signal-to-noise levels) after the upgrade was 10 s. This resolution is fast enough to potentially resolve turbulent eddies in the convective boundary layer; the question was ''Is the accuracy and resolution of state-of-the-art water vapor Raman lidar systems sufficient to derive higher-order moments of turbulence in the boundary layer?'' Wulfmeyer et al. (2010) demonstrated that indeed CARL is able to resolve profiles of the second and third moments of water vapor in the convective boundary layer, and thus variance and skewness profiles can be derived with the accuracy needed to study turbulence. Furthermore, the Raman lidar measurements of water vapor variance and skewness were compared with in situ data collected during the Routine AAF Clouds with Low Optical Water Depths (CLOWD) Optical Radiative Observations (RACORO) field campaign that was conducted over the SGP site during the early part of 2009 (Vogelmann et al. 2012); these results showed good agreement between the two very different techniques (Turner et al. 2014a). The advantage of using an automated system like CARL to study turbulence is that multiple years of data can be included to build a climatology and investigate relationships between different variables (Turner et al. 2014b); this is true for many other processes beyond turbulence.

There are also some new exciting research areas that have resulted from the higher temporal resolution, especially when observations from other instruments are included in the analysis. These include deriving water vapor flux observations using coincident CARL and Doppler lidar measurements, and characterizing entrainment in cumulus clouds using Raman lidar, AERI, cloud radar, microwave radiometer, and surface measurements (Wagner et al. 2013).

e. Current status and future outlook

The primary goal of the Raman lidar within the ARM Program was to provide routine measurements of water vapor through the boundary layer across the diurnal cycle. The original programmatic dream was that water vapor and temperature profile be remotely sensed and that the ARM Program could move away from the routine launching of radiosondes. While the program will probably always need to launch radiosondes to help calibrate the lidar and provide profiles above clouds that attenuate the lidar's laser beam (and provide wind information aloft), the ARM Program has actually realized its dream of using an advanced remote sensor to provide measurements of these key thermodynamic variables at high time and spatial resolution.

The unique and powerful measurements from the SGP Raman lidar have been used in an extremely wide range of research—a much larger range of research than was originally anticipated. This success of the SGP system, both in terms of its operational uptime and its potential to open up new areas of study and contribute to others, led to the decision to build and deploy a new Raman lidar that was almost identical to CARL at the Tropical Western Pacific (TWP) site in Darwin using funds from the American Recovery and Reinvestment Act (ARRA) from 2009. This system became operational in December 2010. Data from this system are already being used to develop climatologies of aerosol extinction and water vapor mixing ratio as a function of synoptic classification, turbulence within the tropical boundary layer, and cirrus cloud macrophysical and optical properties in the tropics where the tropopause is very high (e.g., Thorsen et al. 2013).

The ARM Program took a chance, and invested heavily to advance the Raman lidar technology from a research-only tool into the world's first operational water vapor and aerosol Raman lidar. The success of the ARM Raman lidar enterprise is perhaps best captured in a quote from Reichardt et al. (2012, 8111–8112): ''The Cloud and Radiation Testbed Raman Lidar CARL at the Atmospheric Radiation Measurement program's Southern Great Plains site in Oklahoma stood out because it added another layer of complexity (i.e., it was monitoring tropospheric humidity and clouds continuously and autonomously). Its success enticed meteorological services around the world to develop and operate similar instruments.'' Since that time, the community has seen the development of other automated Raman

lidars (e.g., in Germany, Switzerland, and the Netherlands), but the multiyear record of near continuous observations made by CARL (Fig. 18-2) is totally unique and unprecedented and is clearly one of the shining achievements of the ARM Program.

The ARM Program recently constructed an additional Raman lidar system that was deployed at the new ARM site at Oliktok Point along the northern slope of Alaska in the fall of 2014. Furthermore, the ARM Program recently elected to close its TWP sites, and the Raman lidar at Darwin was relocated to the new ARM site in the Azores in 2015. There will be challenges running these advanced lidar systems in these harsh environments, but we have confidence that these challenges will be overcome and that the scientific benefit will be huge. This will result in three autonomous water vapor and aerosol Raman lidars operating in the ARM Program, which is quite an achievement given the uncertainties surrounding whether a Raman lidar could be made operational in the early 1990s.

Acknowledgments. There have been many people who have contributed to the success of the ARM Raman lidar. The Raman lidar has had a number of different ''instrument mentors'' over its history; these folks have been responsible for overseeing the lidar's operation from a scientific and engineering perspective. Tim Tooman, Rob Newsom, and the authors have all served (or are serving) as mentors for these lidars. We also would like to thank the superb staff at the SGP site, and in particular Chris Martin, as well as the TWP/Darwin staff for routine attention that any lidar system (operational or not) needs. We have benefitted greatly from our interactions with the Raman lidar group at NASA/GSFC over the years, and in particular Harvey Melfi and David Whiteman.

REFERENCES

Ansmann, A., M. Riebesell, and C. Weitkamp, 1990: Measurement of atmospheric aerosol extinction with a Raman lidar. *Opt. Lett.*, **15**, 746–748, doi:10.1364/OL.15.000746.

——, ——, U. Wandinger, C. Weitkamp, E. Voss, W. Lahmann, and W. Michaelis, 1992: Combined Raman elastic backscatter lidar for vertical profiling of moisture, aerosol extinction, backscatter, and lidar ratio. *Appl. Phys.*, **55B**, 18–28, doi:10.1007/BF00348608.

Bisson, S. E., and J. E. M. Goldsmith, 1993: Daytime tropospheric water vapor profile measurements with a Raman lidar. *Opt. Remote Sens. Atmos. Tech. Dig.*, Optical Society of America, 19–22.

——, ——, and M. G. Mitchell, 1999: Narrow-band, narrow-field-of-view Raman lidar with combined day and night capability for tropospheric water-vapor profile measurements. *Appl. Opt.*, **38**, 1841–1849, doi:10.1364/AO.38.001841.

Browell, E. V., T. D. Wilkerson, and T. J. McIlrath, 1979: Water vapor differential absorption lidar development and evaluation. *Appl. Opt.*, **18**, 3474–3483, doi:10.1364/AO.18.003474.

——, and Coauthors, 1997: LASE validation experiment. *Advances in Atmospheric Remote Sensing with Lidar*, A. Ansmann et al., Eds., Springer-Verlag, 289–295.

Campbell, J. R., D. L. Hlavka, E. J. Welton, C. J. Flynn, D. D. Turner, J. D. Spinhirne, V. S. Scott, and I. H. Hwang, 2002: Full-time, eye-safe cloud and aerosol lidar observations at Atmospheric Radiation Measurement Program sites: Instruments and data processing. *J. Atmos. Oceanic Technol.*, **19**, 431–442, doi:10.1175/1520-0426(2002)019<0431:FTESCA>2.0.CO;2.

Comstock, J. M., T. P. Ackerman, and D. D. Turner, 2004: Evidence of high ice supersaturation in cirrus clouds using ARM Raman lidar measurements. *Geophys. Res. Lett.*, **31**, L11106, doi:10.1029/2004GL019705.

Cooney, J. A., 1968: Measurements on the Raman component of laser atmospheric backscatter. *Appl. Phys. Lett.*, **12**, 40, doi:10.1063/1.1651884.

Di Girolamo, P., R. Marchese, D. N. Whiteman, and B. B. Demoz, 2004: Rotational Raman lidar measurements of atmospheric temperature in the UV. *Geophys. Res. Lett.*, **31**, L01106, doi:10.1029/2003GL018342.

DOE, 1990: Atmospheric Radiation Measurement Program Plan. U.S. Department of Energy Rep. DOE/ER-0441, 121 pp.

Ehret, G., C. Kiemle, W. Renger, and G. Simmet, 1993: Airborne remote sensing of tropospheric water vapor with a near-infrared differential absorption lidar system. *Appl. Opt.*, **32**, 4534–4551, doi:10.1364/AO.32.004534.

Ferrare, R. A., S. H. Melfi, D. N. Whiteman, K. D. Evans, F. J. Schmidlin, and D. O'C. Starr, 1995: A comparison of water vapor measurements made by Raman lidar and radiosondes. *J. Atmos. Oceanic Technol.*, **12**, 1177–1195, doi:10.1175/1520-0426(1995)012<1177:ACOWVM>2.0.CO;2.

——, D. D. Turner, L. A. Heilman Brasseur, W. F. Feltz, O. Dubovik, and T. P. Tooman, 2001: Raman lidar observations of the aerosol extinction-to-backscatter ratio over the southern Great Plains. *J. Geophys. Res.*, **106**, 20 333–20 348, doi:10.1029/2000JD000144.

——, and Coauthors, 2004: Characterization of upper-tropospheric water vapor measurements during AFWEX using LASE. *J. Atmos. Oceanic Technol.*, **21**, 1790–1808, doi:10.1175/JTECH-1652.1.

——, and Coauthors, 2006: Evaluation of daytime measurements of aerosols and water vapor made by an operational Raman lidar over the southern Great Plains. *J. Geophys. Res.*, **111**, D05S08, doi:10.1029/2005JD005836.

Ghan, S. J., and Coauthors, 2006: Use of in situ cloud condensation nuclei, extinction, and aerosol size distribution measurements to test a method for retrieving cloud condensation nuclei profiles from surface measurements. *J. Geophys. Res.*, **111**, D05S10, doi:10.1029/2004JD005752.

Goldsmith, J. E. M., and R. A. Ferrare, 1992: Performance modeling of daytime Raman lidar systems for profiling atmospheric water vapor. Sixteenth International Laser Radar Conference Proceedings, M. P. McCormick, Ed., NASA Publ. 3158, Part 2, 667–670.

——, S. E. Bisson, R. A. Ferrare, K. D. Evans, D. N. Whiteman, and S. H. Melfi, 1994: Raman lidar profiling of atmospheric water vapor: Simultaneous measurements with two collocated systems. *Bull. Amer. Meteor. Soc.*, **75**, 975–982, doi:10.1175/1520-0477(1994)075<0975:RLPOAW>2.0.CO;2.

——, F. H. Blair, S. E. Bisson, and D. D. Turner, 1998: Turn-key Raman lidar for profiling atmospheric water vapor, clouds,

and aerosols. *Appl. Opt.*, **37**, 4979–4990, doi:10.1364/AO.37.004979.

Grant, W. B., 1991: Differential absorption and Raman lidar for water vapor profile measurements: A review. *Opt. Eng.*, **30**, 40–48, doi:10.1117/12.55772.

Ismail, S., and E. V. Browell, 1989: Airborne and spaceborne lidar measurements of water vapor profiles: A sensitivity analysis. *Appl. Opt.*, **28**, 3603–3615, doi:10.1364/AO.28.003603.

Kato, S., and Coauthors, 2000: A comparison of the aerosol optical thickness derived from ground-based and airborne measurements. *J. Geophys. Res.*, **105**, 14 701–14 717, doi:10.1029/2000JD900013.

Leonard, D. A., 1967: Observation of Raman scattering from the atmosphere using a pulsed nitrogen ultraviolet laser. *Nature*, **216**, 142–143, doi:10.1038/216142a0.

Linne, H., D. D. Turner, J. E. M. Goldsmith, T. P. Tooman, J. Bösenberg, K. Ertel, and S. Lehmann, 2000: Intercomparison of DIAL and Raman lidar measurements of humidity profiles. *Advances in Laser Remote Sensing: Selected Papers Presented at the 20th International Laser Radar Conference,* D. Dabas, C. Loth, and J. Pelon, Eds., Ecole Polytechnique, 293–298.

Masonis, S. J., K. Franke, A. Ansmann, D. Müller, D. Althausen, J. A. Ogren, A. Jefferson, and P. J. Sheridan, 2002: An intercomparison of aerosol light extinction and 180° backscatter as derived using in situ instruments and Raman lidar during the INDOEX field campaign. *J. Geophys. Res.*, **107**, 8014, doi:10.1029/2000JD000035.

McComiskey, A., and R. A. Ferrare, 2016: Aerosol physical and optical properties and processes in the ARM Program. *The Atmospheric Radiation Measurement (ARM) Program: The First 20 Years*, *Meteor. Monogr.*, No. 57, Amer. Meteor. Soc., doi:10.1175/AMSMONOGRAPHS-D-15-0028.1.

Mecikalski, J. R., K. M. Bedka, D. D. Turner, W. F. Feltz, and S. J. Peach, 2006: Ability to quantify coherent turbulent structures in the convective boundary layer using thermodynamic profiling instruments. *J. Geophys. Res.*, **111**, D12203, doi:10.1029/2005JD006456.

Melfi, S. H., 1972: Remote measurement of the atmosphere using Raman scattering. *Appl. Opt.*, **11**, 1605–1610, doi:10.1364/AO.11.001605.

——, D. N. Whiteman, and R. A. Ferrare, 1989: Observation of atmospheric fronts using Raman lidar moisture measurements. *J. Appl. Meteor.*, **28**, 789–806, doi:10.1175/1520-0450(1989)028<0789:OOAFUR>2.0.CO;2.

——, K. D. Evans, J. Li, D. N. Whiteman, R. A. Ferrare, and G. Schwemmer, 1997: Observations of Raman scattering by cloud droplets in the atmosphere. *Appl. Opt.*, **36**, 3551–3559, doi:10.1364/AO.36.003551.

Newsom, R. K., D. D. Turner, B. Mielke, M. Clayton, R. A. Ferrare, and C. Sivaraman, 2009: The use of simultaneous analog and photon counting detection for Raman lidar. *Appl. Opt.*, **48**, 3903–3914, doi:10.1364/AO.48.003903.

——, ——, and J. E. M. Goldsmith, 2013: Long-term evaluation of temperature profiles measured by an operational Raman lidar. *J. Atmos. Oceanic Technol.*, **30**, 1616–1634, doi:10.1175/JTECH-D-12-00138.1.

Pahlow, M., and Coauthors, 2006: Comparison between lidar and nephelometer measurements of aerosol hygroscopicity at the Southern Great Plains Atmospheric Radiation Measurement site. *J. Geophys. Res.*, **111**, D05S15, doi:10.1029/2004JD005646.

Peppler, R. A., and Coauthors, 2000: ARM Southern Great Plains observations of the smoke pall associated with the 1998 Central American fires. *Bull. Amer. Meteor. Soc.*, **81**, 2563–2591, doi:10.1175/1520-0477(2000)081<2563:ASGPSO>2.3.CO;2.

Reichardt, J., U. Wandinger, M. Serwazi, and C. Weitkamp, 1996: Combined Raman lidar for aerosol, ozone, and moisture measurements. *Opt. Eng.*, **35**, 1457–1465, doi:10.1117/1.600681.

——, ——, V. Klein, I. Mattis, B. Hilber, and R. Begbie, 2012: RAMSES: German meteorological service autonomous Raman lidar for water vapor, temperature, aerosol, and cloud measurements. *Appl. Opt.*, **51**, 8111–8131, doi:10.1364/AO.51.008111.

Renaut, D., J. C. Pourney, and R. Capitani, 1980: Daytime Raman-lidar measurements of water vapor. *Opt. Lett.*, **5**, 233–235, doi:10.1364/OL.5.000233.

Revercomb, H. E., and Coauthors, 2003: The ARM Program's water vapor intensive observations periods: Overview, initial accomplishments, and future challenges. *Bull. Amer. Meteor. Soc.*, **84**, 217–236, doi:10.1175/BAMS-84-2-217.

Sakai, T., D. N. Whiteman, F. Russo, D. D. Turner, I. Veselovskii, S. H. Melfi, and T. Nagai, 2013: Liquid water cloud measurements using the Raman lidar technique: Current understanding and future research needs. *J. Atmos. Oceanic Technol.*, **30**, 1337–1353, doi:10.1175/JTECH-D-12-00099.1.

Schmid, B., and Coauthors, 2006: How well do state-of-the-art techniques measuring the vertical profile of tropospheric aerosol extinction compare? *J. Geophys. Res.*, **111**, D05S07, doi:10.1029/2005JD005837.

Smullin, L. D., and G. Fiocco, 1962: Optical echoes from the moon. *Nature*, **194**, 1267, doi:10.1038/1941267a0.

Soden, B. J., S. A. Ackerman, D. O'C. Starr, S. H. Melfi, and R. A. Ferrare, 1994: Comparison of upper tropospheric water vapor from GOES, Raman lidar, and cross-chain loran atmospheric sounding system measurements. *J. Geophys. Res.*, **99**, 21 005–21 016, doi:10.1029/94JD01721.

——, D. D. Turner, B. M. Lesht, and L. M. Miloshevich, 2004: An analysis of satellite, radiosonde, and lidar observations of upper tropospheric water vapor from the Atmospheric Radiation Measurement Program. *J. Geophys. Res.*, **109**, D04105, doi:10.1029/2003JD003828.

Stokes, G. M., 2016: Original ARM concept and launch. *The Atmospheric Radiation Measurement (ARM) Program: The First 20 Years*, *Meteor. Monogr.*, No. 57, Amer. Meteor. Soc., doi:10.1175/AMSMONOGRAPHS-D-15-0021.1.

Thorsen, T. J., Q. Fu, J. M. Comstock, C. Sivaraman, M. A. Vaughn, D. M. Winker, and D. D. Turner, 2013: Macrophysical properties of tropical cirrus clouds from the CALIPSO satellite and from ground-based micropulse and Raman lidars. *J. Geophys. Res. Atmos.*, **118**, 9209–9220, doi:10.1002/jgrd.50691.

Turner, D. D., and J. E. M. Goldsmith, 1999: Twenty-four-hour Raman lidar water vapor measurements during the Atmospheric Radiation Measurement Program's 1996 and 1997 water vapor intensive observations periods. *J. Atmos. Oceanic Technol.*, **16**, 1062–1076, doi:10.1175/1520-0426(1999)016<1062:TFHRLW>2.0.CO;2.

——, and D. N. Whiteman, 2002: Remote Raman spectroscopy. Profiling water vapor and aerosols in the troposphere using Raman lidars. *Handbook of Vibrational Spectroscopy*, Vol. 4, J. M. Chalmers and P. R. Griffiths, Eds., Wiley and Sons, 2857–2878.

——, W. F. Feltz, and R. A. Ferrare, 2000: Continuous water vapor profiles from operational ground-based active and passive remote sensors. *Bull. Amer. Meteor. Soc.*, **81**, 1301–1317, doi:10.1175/1520-0477(2000)081<1301:CWBPFO>2.3.CO;2.

——, R. A. Ferrare, and L. A. Brasseur, 2001: Average aerosol extinction and water vapor profiles over the southern Great Plains. *Geophys. Res. Lett.*, **28**, 4441–4444, doi:10.1029/2001GL013691.

——, ——, L. A. Heilman Brasseur, W. F. Feltz, and T. P. Tooman, 2002: Automated retrieval of water vapor and aerosol profiles from an operational Raman lidar. *J. Atmos. Oceanic Technol.*, **19**, 37–50, doi:10.1175/1520-0426(2002)019<0037:AROWVA>2.0.CO;2.

——, B. M. Lesht, S. A. Clough, J. C. Liljegren, H. E. Revercomb, and D. C. Tobin, 2003: Dry bias and variability in Vaisala radiosondes: The ARM experience. *J. Atmos. Oceanic Technol.*, **20**, 117–132, doi:10.1175/1520-0426(2003)020<0117:DBAVIV>2.0.CO;2.

——, and Coauthors, 2004: The QME AERI LBLRTM: A closure experiment for downwelling high spectral resolution infrared radiance. *J. Atmos. Sci.*, **61**, 2657–2675, doi:10.1175/JAS3300.1.

——, R. A. Ferrare, V. Wulfmeyer, and A. J. Scarino, 2014a: Aircraft evaluation of ground-based Raman lidar water vapor turbulence profiles in convective mixed layers. *J. Atmos. Oceanic Technol.*, **31**, 1078–1088, doi:10.1175/JTECH-D-13-00075.1.

——, V. Wulfmeyer, L. K. Berg, and J. H. Schween, 2014b: Water vapor turbulence profiles in stationary continental convective mixed layers. *J. Geophys. Res. Atmos.*, **119**, 11 151–11 165, doi:10.1002/2014JD022202.

——, E. J. Mlawer, and H. E. Revercomb, 2016: Water vapor observations in the ARM Program. *The Atmospheric Radiation Measurement (ARM) Program: The First 20 Years*, *Meteor. Monogr.*, No. 57, Amer. Meteor. Soc., doi:10.1175/AMSMONOGRAPHS-D-15-0025.1.

Vogelmann, A. M., and Coauthors, 2012: RACORO extended-term aircraft observations of boundary layer clouds. *Bull. Amer. Meteor. Soc.*, **93**, 861–878, doi:10.1175/BAMS-D-11-00189.1.

Wagner, T. J., D. D. Turner, L. K. Berg, and S. K. Krueger, 2013: Ground-based remote retrievals of cumulus entrainment rates. *J. Atmos. Oceanic Technol.*, **30**, 1460–1471, doi:10.1175/JTECH-D-12-00187.1.

Wang, Z., D. N. Whiteman, B. B. Demoz, and I. Veselovskii, 2004: A new way to measure cirrus cloud ice water content by using ice Raman scatter with Raman lidar. *Geophys. Res. Lett.*, **31**, L15101, doi:10.1029/2004GL020004.

Weckwerth, T. M., V. Wulfmeyer, R. M. Wakimoto, R. M. Hardesty, J. W. Wilson, and R. M. Banta, 1999: NCAR–NOAA lower-tropospheric water vapor workshop. *Bull. Amer. Meteor. Soc.*, **80**, 2339–2357, doi:10.1175/1520-0477(1999)080<2339:NNLTWV>2.0.CO;2.

Whiteman, D. N., and S. H. Melfi, 1999: Cloud liquid water, mean droplet radius, and number density measurements using a Raman lidar. *J. Geophys. Res.*, **104**, 31 411–31 419, doi:10.1029/1999JD901004.

——, ——, and R. A. Ferrare, 1992: Raman lidar system for the measurement of water vapor and aerosols in the Earth's atmosphere. *Appl. Opt.*, **31**, 3068–3082, doi:10.1364/AO.31.003068.

——, ——, R. A. Campbell, and K. D. Evans, 1993: Solar blind Raman scattering measurements of water vapor using a KrF excimer laser. *Opt. Remote Sens. Atmos. Tech. Dig.*, Optical Society of America, 165–168.

——, and Coauthors, 2006: Raman lidar measurements during the international H_2O project. Part I: Instrumentation and analysis techniques. *J. Atmos. Oceanic Technol.*, **23**, 157–169, doi:10.1175/JTECH1838.1.

Wulfmeyer, V., and J. Bösenberg, 1998: Ground-based differential absorption lidar for water vapor profiling: Assessment of accuracy, resolution, and meteorological applications. *Appl. Opt.*, **37**, 3825–3844, doi:10.1364/AO.37.003825.

——, S. Pal, D. D. Turner, and E. Wagner, 2010: Can water vapour Raman lidar resolve profiles of turbulent variables in the convective boundary layer? *Bound.-Layer Meteor.*, **136**, 253–284, doi:10.1007/s10546-010-9494-z.